JOURNAL OF Materials CHEMISTRY

Doping studies of the ferromagnetic superconductor $RuSr_2GdCu_2O_8$†

A. C. Mclaughlin,[a,b] V. Janowitz,[a,b] J. A. McAllister[a,b] and J. P. Attfield*[a,b]

[a]*Department of Chemistry, University of Cambridge, Lensfield Road, Cambridge, UK CB2 1EW*
[b]*Interdisciplinary Research Centre in Superconductivity, University of Cambridge, Madingley Road, Cambridge, UK CB3 0HE*

Received 24th May 2000, Accepted 29th June 2000
First published as an Advance Article on the web TBC

Solid solutions of the ferromagnetic superconductor $Ru_{1-x}M_xSr_2GdCu_2O_8$ have been prepared for M = Sn or Nb. Up to 7.5% Sn and 20% Nb have been incorporated into the structure, and powder diffraction and physical measurements show that substitution occurs at the Ru site. A suppression of the ferromagnetic moment in the ruthenate layers is observed upon Sn and Nb substitution and the Curie temperature drops from 136 K in the undoped material to 103 K in $Ru_{0.8}Nb_{0.2}Sr_2GdCu_2O_8$. The onset of superconductivity increases from 19 K in the 15% Nb doped sample to 38 K in the parent compound to 50 K in the 7.5% Sn doped sample, evidencing a tuning of the superconducting transition by charge transfer. Structural changes upon M doping have been determined from powder synchrotron X-ray diffraction and, for one sample, neutron diffraction using the high flux diffractometer GEM to compensate for the high absorption of natural Gd.

Introduction

Superconductivity and ferromagnetism are important and useful properties, but they do not usually coexist in the same material. This is borne out by several re-entrant superconductors in which the onset of ferromagnetic ordering destroys the superconductivity; for example $ErRh_4B_4$ exhibits a superconducting transition at 8.7 K and orders ferromagnetically at $T_M = 0.93$ K, with the simultaneous disappearance of the superconducting state.[1] However, a coexistence of ferromagnetism and superconductivity has recently been observed in the 1212 type layered cuprate $RuSr_2GdCu_2O_8$,[2–10] which is a bulk superconductor below $T_c = 0$–46 K. The magnetic transition at $T_M = 136$ K results from the ordering of moments in the RuO_2 planes and persists through the onset of superconductivity to the lowest temperature investigated (1.9 K). A variety of physical measurements, in particular zero-field muon spin rotation experiments,[6] have demonstrated that the material is isotropically uniform with no evidence of spatial separation of the superconducting and magnetic regions. The presence of ferromagnetism is confirmed by the observation of hysteresis loops in variable field measurements below T_M, with remnant and saturated moments of 0.1 and 1.0 μ_B per Ru atom. However, only antiferromagnetic order within the RuO_2 planes was detected in a recent neutron scattering experiment and the ferromagnetism is proposed to arise from a spin flop transition at high fields.[8] The Gd moments align antiferromagnetically, but at much lower temperatures ($T_N = 2.9$ K).

The average crystal structure of $RuSr_2GdCu_2O_8$ is tetragonal with *P4/mmm* space group symmetry and the structure is similar to that of other 1212-type cuprate superconductors, consisting of a layer of almost regular RuO_6 octahedra connected through their apices to two layers of CuO_5 square pyramids (Fig. 1). There is a bond mismatch between the in-plane Ru–O and Cu–O bonds leading to rotations of the RuO_6 octahedra around *c* by 13° at 295 K. A slight tilting of the polyhedra which reduces the Cu–O–Ru angle to 173° is also observed.[7,9] A slight canting of the moments may arise from an antisymmetric (Dzyaloshinsky–Moriya) interaction between neighbouring Ru moments, which is non-zero due to the twists and tilts of the RuO_6 octahedra. This would give rise to an overall magnetic arrangement containing both ferro- and antiferromagnetic components, in keeping with the above magnetic observations.

$RuSr_2GdCu_2O_8$ is found to be both cation and oxygen

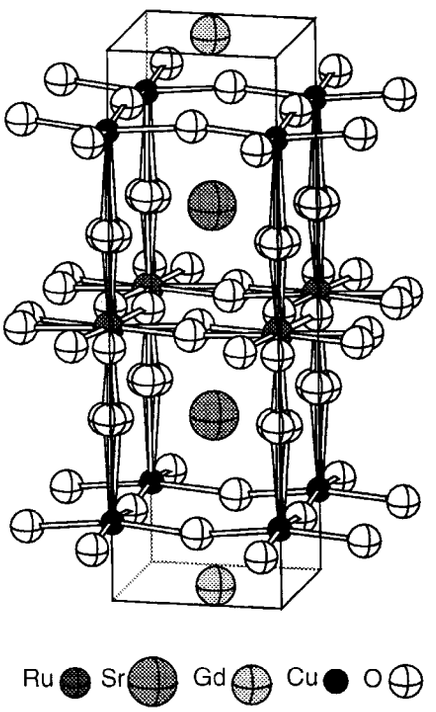

Fig. 1 The average crystal structure of $RuSr_2GdCu_2O_8$ showing the tilts and rotations of the RuO_6 octahedra.

†Basis of a presentation given at Materials Discussion No. 3, 26–29 September, 2000, University of Cambridge, UK.

DOI: 10.1039/b002952l

Table 1 Refined atomic parameters for $Ru_{1-x}M_xSr_2GdCu_2O_8$ solid solutions using synchrotron and neutron (N) radiations for the M = Sn samples and laboratory X-ray diffraction data for M = Nb. Atom positions are Ru 1(b) (0, 0, 1/2), Sr 2(h) (1/2, 1/2, z), Gd 1(c) (1/2, 1/2, 0), Cu 2(g) (0, 0, z), O(1) 8(s) (x, 0, z), O(2) 4(i) (0, 1/2, z), O(3) 4(o) (x, 1/2, 0)

			% Sn				% Nb				
Atom	Occupancy		0	5	5 (N)	7.5	0	5	10	15	20
Ru	1.00	U_{iso}/Å^2	0.0037(2)	0.0039(2)	0.0071(85)	0.0046(2)	0.0003(3)	0.0034(3)	0.0027(2)	0.021(2)	0.0068(5)
Sr	1.00	z	0.30926(6)	0.30873(7)	0.3031(12)	0.30877(8)	0.3105(1)	0.3099(1)	0.3086(1)	0.3084(1)	0.3072(2)
		U_{iso}/Å^2	0.0084(1)	0.0079(2)	0.0071	0.0086(2)	0.00030	0.0034	0.0027	0.0021	0.0068
Gd	1.00	U_{iso}/Å^2	0.0046(1)	0.0045(1)	0.0071	0.0046(2)	0.00030	0.0034	0.0027	0.0021	0.0068
Cu	1.00	z	0.14611(9)	0.14607(9)	0.1511(12)	0.1458(1)	0.1475(2)	0.1473(2)	0.147(2)	0.1463(2)	0.1470(5)
		U_{iso}/Å^2	0.0052(2)	0.0051(2)	0.0071	0.0053(2)	0.00030	0.0034	0.0027	0.0021	0.0068
O(1)	0.25	x	0.049(3)	0.054(3)	0.030(13)	0.042(5)	0.063(7)	0.04(2)	0.079(5)	0.074(6)	0.080(1)
		z	0.3332(4)	0.3340(4)	0.3356(16)	0.3331(5)	0.3318(9)	0.3337(9)	0.3350(8)	0.3360(9)	0.3360(9)
		U_{iso}/Å^2	0.0127(7)	0.0120(7)	0.0071	0.0155(9)	−0.012(2)	−0.012(2)	−0.012(2)	−0.015(3)	−0.011(3)
O(2)	1.00	z	0.1304(3)	0.1308(3)	0.1239(10)	0.1304(3)	0.1339(6)	0.1302(5)	0.1335(5)	0.1345(6)	0.1330(9)
		U_{iso}/Å^2	0.0127(7)	0.0120(7)	0.0071	0.0155(9)	−0.012	−0.012	−0.012	−0.015	−0.011
O(3)	0.50	x	0.113(2)	0.116(2)	0.1183(59)	0.120(2)	0.133(4)	0.138(4)	0.137(3)	0.148(4)	0.1621(5)
		U_{iso}/Å^2	0.0127(7)	0.0120(7)	0.0071	0.0155(9)	−0.012	−0.012	−0.012	−0.015	−0.011

stoichiometric[7] and the hole doping of the copper oxide planes necessary to induce superconductivity arises from the overlap of the Ru: t_{2g} and the Cu: $3d_{x^2-y^2}$ bands. The formula may be written as $Ru^{5-2p_0}Sr_2Gd(Cu^{2+p_0})_2O_8$ to show the average Ru and Cu oxidation states. Transport measurements suggest that the copper oxide planes in $RuSr_2GdCu_2O_8$ are underdoped with intrinsic hole doping level $p_0 = 0.07$[6] as optimum superconductivity in the layered cuprates is generally found at $p_0 = 0.16$. In order to investigate the charge distribution and magnetisation of $RuSr_2GdCu_2O_8$ further, we have attempted to replace Ru by non-magnetic, fixed valent cations. The substitution of the larger Sn^{4+} ion for Ru was previously found to increase the bond mismatch between the in plane Ru–O and Cu–O bonds, and enhanced T_c but suppressed T_M.[11] However, firm conclusions about the origin of these effects could not be made because the samples were impure. A series of phase pure Sn-doped samples for $x < 0.1$ and a series of >98% pure Nb doped samples have subsequently been prepared and characterised by X-ray diffraction, room temperature thermopower measurements, SQUID magnetometry and conductivity measurements. A summary of the physical properties of these materials has been reported elsewhere.[12]

Experimental

Ceramic samples of nominal composition $Ru_{1-x}M_xSr_2GdCu_2O_8$ (M = Sn: $x = 0$, 0.025, 0.05, 0.075; M = Nb: $x = 0$, 0.05, 0.1, 0.15, 0.2) were prepared by the solid state reaction of stoichiometric powders of RuO_2, SnO_2, Nb_2O_5, $SrCO_3$, Gd_2O_3, and CuO. These were ground and die-pressed into pellets before preliminary reaction in flowing nitrogen at 1010 °C for 20 hours in order to minimise the formation of $SrRuO_3$. This was followed by reaction in flowing oxygen at 1050 °C and 1055 °C for 10 hours each. The sample was furnace cooled, reground and repelleted between each step. The samples were annealed at 1060 °C under flowing oxygen for 4 days and finally slow cooled to room temperature. X-Ray diffraction patterns demonstrated that the $Ru_{1-x}Sn_xSr_2GdCu_2O_8$ solid solutions were phase pure, however there was a trace (<2%) of $SrRuO_3$ in the $Ru_{1-x}Nb_xSr_2GdCu_2O_8$ samples. Thermogravimetric analyses under flowing H_2/N_2 showed the samples to have oxygen contents of 8.00 ± 0.05%, and so they are oxygen stoichiometric within the limits of the measurements.

Room temperature X-ray diffraction data were collected for the $Ru_{1-x}Nb_xSr_2GdCu_2O_8$ solid solutions on a high resolution STOE transmission diffractometer using Cu $K\alpha_1$ radiation. The counter is a moving linear position sensitive detector with a resolution of <0.06° FWHM (Full Width at Half Maximum) in 2θ. Data were collected over the range $5° < 2\theta < 100°$, with a step size of 0.01°. Powder synchrotron X-ray diffraction patterns of the $Ru_{1-x}Sn_xSr_2GdCu_2O_8$ solid solutions ($x = 0$, 0.05, 0.075) were recorded on ESRF instrument BM16 at 295 K.[13] A wavelength of 0.325104 Å was used and the sample was contained in a 0.5 mm diameter borosilicate glass capillary mounted on the axis of the diffractometer about which it was spun at 1 Hz to improve the powder averaging of the

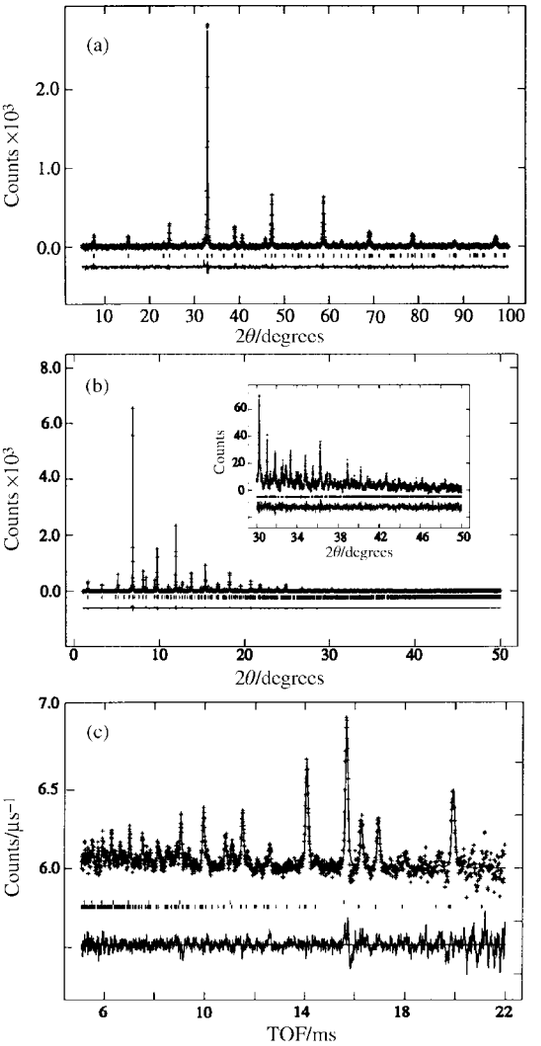

Fig. 2 Rietveld refinement fits to (a) the Cu $K\alpha_1$ X-ray diffraction pattern of $Ru_{0.8}Nb_{0.2}Sr_2GdCu_2O_8$, (b) the synchrotron X-ray diffraction pattern of $Ru_{0.95}Sn_{0.05}Sr_2GdCu_2O_8$ and (c) the TOF neutron diffraction pattern of $Ru_{0.95}Sn_{0.05}Sr_2GdCu_2O_8$.

crystallites. Diffraction patterns were collected over the angular range 2–50° by continuously scanning the bank of nine Ge(111) analyser crystals and scintillation detectors at a rate of 1 degree per minute and recording data every 100 ms. The high-angle parts of the pattern were scanned several times to improve the statistical quality of the data in these regions. The counts from the nine detectors were then normalised, summed and rebinned to a constant step size of 0.004° for each scan.

Time-of-flight (TOF) neutron powder diffraction data were collected on the General Materials Diffractometer (GEM) of the ISIS facility at the Rutherford-Appleton Laboratory, UK for the $Ru_{0.95}Sn_{0.05}Sr_2GdCu_2O_8$ sample. GEM has been designed as a high intensity, high-resolution neutron diffractometer for structural studies of disordered materials and crystalline powders and has an incident flight path of 17 m. A cylindrical sample was prepared to allow for the extremely high absorption cross section of Gd for thermal neutrons by coating a cylinder of adhesive tape (approximate dimensions 6.1×0.6 cm) with a 0.05 mm layer of $Ru_{0.95}Sn_{0.05}Sr_2GdCu_2O_8$ powder. This cylinder was held in a vanadium can and room temperature diffraction patterns were collected over the range 1000–22000 μs in 24 h from the 20, 60, and 90° 2θ detector banks.

Magnetisations were measured on powdered samples in a Quantum Design SQUID magnetometer. The resistivities of sintered polycrystalline bars (approximate dimensions $4 \times 4 \times 12$ mm^3) were measured between 7 and 300 K using the standard four-probe ac technique. The thermoelectric powers of the same sintered bars were measured at 290 K using the method and instrument developed by Obertelli *et al.*,[14] and were corrected for the contribution from the gold connecting leads which was measured separately using a Pb standard.

Results

The X-ray and TOF neutron powder diffraction patterns were all fitted by the Rietveld method[15] using a GSAS program[16] with the starting model previously reported for $RuSr_2GdCu_2O_8$.[7] The backgrounds were fitted using linear interpolation and the peak shapes were modelled using a pseudo-Voigt function. The oxygen sites of the RuO_6 octahedra are split to model the disordered rotations and tilts of the octahedra (Table 1). Good Rietveld fits were obtained for all samples (Fig. 2).

Refinement of the internal co-ordinates in the $Ru_{1-x}Nb_xSr_2GdCu_2O_8$ solid solutions reveals increases in the average in-plane Ru–O (Fig. 3) and Sr–O bonds (Table 2) and an increase of the rotations of the RuO_6 octahedra around c. Overall increases in the lattice parameters (Table 2) and cell volume (Fig. 4) are also observed in accordance with the substitution of the slightly larger Nb^{5+} for $Ru^{4+/5+}$. The observation of an increase in the apical Cu–O bond distance with Nb substitution (Fig. 5) is indicative of a reduction in hole transfer from the ruthenate to the cuprate layers, in keeping with the transport properties below.

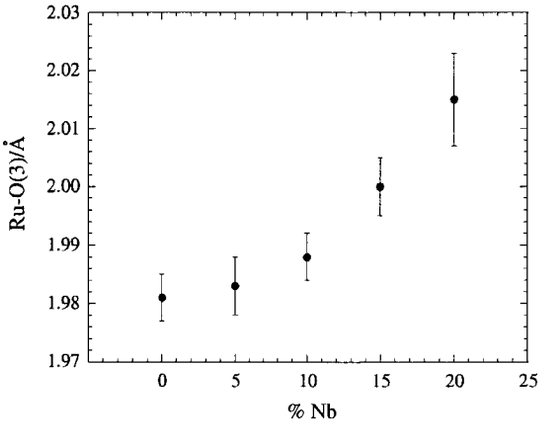

Fig. 3 Variation of the in-plane Ru–O bond with x in the $Ru_{1-x}Nb_xSr_2GdCu_2O_8$ solid solutions.

A previous study showed that the substitution of Sn into $RuSr_2GdCu_2O_8$[11] increases the a cell parameter, while c decreases leading to no overall change in the cell volume. Refinement of the cell parameters from more highly-resolved synchrotron data confirms the increase in the a cell parameter but an expansion of c and cell volume are observed (Table 2), as expected for the substitution of the larger Sn^{4+} ion for $Ru^{4+/5+}$. The increase of the in-plane Ru–O bond and the concomitant decrease in Ru–O–Ru angle detected in the previous study are also observed, however clear trends in the Cu–O distances are not seen in these results.

An acceptable Rietveld refinement of the structure of $Ru_{0.95}Sn_{0.05}Sr_2GdCu_2O_8$ was obtained by fitting the neutron diffraction data from the 90° bank of GEM (Fig. 2(c)). The data were corrected for Gd absorption, varying as TOF, and reflections from the vanadium can were fitted as a secondary phase. Free refinement of the atomic coordinates was possible although all of the isotropic thermal factors were constrained to be equal. The atomic positions, bond distances and angles

Table 2 Bond lengths (Å) and angles (°), cell parameters, and agreement factors from the refinements of $Ru_{1-x}M_xSr_2GdCu_2O_8$ solid solutions

	% Sn				% Nb				
	0	5	5 (N)	7.5	0	5	10	15	20
Cu–O(1) × 1	2.174(5)	2.186(5)	2.14(2)	2.176(6)	2.13(1)	2.16(1)	2.19(1)	2.21(1)	2.21(2)
Cu–O(2) × 4	1.9284(3)	1.9289(3)	1.945(3)	1.9290(4)	1.920(1)	1.924(1)	1.921(1)	1.920(1)	1.925(1)
Sr–O(1) × 2	2.601(9)	2.591(8)	2.66(3)	2.620(9)	2.55(2)	2.61(3)	2.52(1)	2.53(1)	2.52(2)
Sr–O(1) × 2	2.864(9)	2.881(9)	2.82(4)	2.847(9)	2.89(2)	2.83(4)	2.94(1)	2.93(1)	2.96(3)
Sr–O(2) × 4	2.823(3)	2.817(3)	2.83(1)	2.821(3)	2.796(6)	2.830(6)	2.785(5)	2.775(5)	2.780(9)
Sr–O(3) × 2	2.661(4)	2.660(4)	2.71(2)	2.652(4)	2.596(9)	2.597(9)	2.605(7)	2.586(8)	2.576(15)
Sr–O(3) × 2	3.226(5)	3.242(5)	3.29(2)	3.254(6)	3.26(1)	3.27(1)	3.29(1)	3.33(1)	3.37(3)
Ru–O(1) × 2	1.939(5)	1.933(5)	1.91(2)	1.940(6)	1.96(1)	1.94(1)	1.93(1)	1.91(1)	1.91(2)
Ru–O(3) × 4	1.968(1)	1.972(2)	1.972(5)	1.976(2)	1.981(4)	1.983(5)	1.988(4)	2.000(5)	2.015(9)
Cu–O(1)–Ru	169.5(1)	168.5(7)	174(3)	171.0(9)	166(2)	170(2)	163(1)	164(1)	163(3)
Cu–O(2)–Cu	169.2(2)	169.5(2)	162(2)	169.4(3)	170.6(5)	171.0(7)	170.7(5)	171.9(5)	170.4(9)
Ru–O(3)–Ru	154.6(4)	153.8(4)	153(1)	152.9(5)	150.9(9)	149.7(9)	148.9(8)	146.6(9)	144.1(9)
a/Å	3.83955(1)	3.84157(1)	3.8388(6)	3.84162(1)	3.82765(5)	3.82828(6)	3.83083(4)	3.83188(5)	3.83840(2)
c/Å	11.57239(7)	11.58011(8)	11.571(3)	11.58258(7)	11.5365(2)	11.5356(3)	11.5408(2)	11.5432(2)	11.5444(8)
V/Å^3	170.602(11)	170.895(1)	170.51(1)	170.936(1)	169.020(8)	169.062(8)	169.364(6)	169.492(8)	169.69(1)
χ^2	2.0	1.9	1.0	1.4	1.2	1.4	1.5	1.4	1.0
R_{WP} (%)	8.9	9.0	0.3	10.5	2.8	3.0	2.8	3.0	6.2
R_P (%)	6.4	6.5	0.3	7.7	3.6	3.9	2.8	3.0	7.9

(Tables 1 and 2) from this refinement are in good agreement with those from the synchrotron X-ray refinement of the same structure, within the usual criterion of three e.s.d.s (estimated standard deviations), and the neutron e.s.d.s on the oxygen positions and metal to oxygen distances are only 4–5 times larger than those for the synchrotron refinement. These results demonstrate that powder neutron structure determination of materials containing significant quantities of natural Gd is now possible because of the very high flux offered by diffractometers such as GEM. The future addition of backscattering detector banks should yield even better refinements from this instrument.

A reduction of the Curie temperature (T_M) and a broadening of the magnetic transition is clearly observed in magnetisation data for both the Sn and Nb substituted materials (Fig. 6), collected while warming in an applied field of 1 kOe after zero-field cooling. Magnetic hysteresis loops recorded at 10 K with the field swept between ± 50 kOe confirm that there is a ferromagnetically ordered component in all the samples; a typical loop is displayed in Fig. 7. The remnant moment and coercive field decrease smoothly with x for both $Ru_{1-x}Sn_xSr_2GdCu_2O_8$ and $Ru_{1-x}Nb_xSr_2GdCu_2O_8$ series (Table 3). Both the Ru moment μ_{Ru} and the paramagnetic Gd moment μ_{Gd} contribute to the overall magnetisation. The saturated Ru moment was estimated by fitting the total magnetic moment $\mu(H)$ in the range $H=25$–50 kOe with the function:

$$\mu(H)=\mu_{Gd}F(H)+(1-x)\mu_{Ru}$$

where $F(H)$ is the Brillouin function for the $S=7/2$ Gd^{3+} spins. The estimated Ru moment decreases rapidly with x for both the Sn and Nb substituted samples (Table 3).

The Meissner state is evidenced by measuring magnetisations in a field of 2 Oe, after zero-field cooling. Data were collected for the $Ru_{1-x}Sn_xSr_2GdCu_2O_8$ solid solutions as shown in Fig. 6(c). The T_c's measured from the onset of diamagnetism are in good agreement with the zero-resistance values obtained from resistivity measurements (Table 2). The Curie transitions are indicated by small maxima in the susceptibilities, at the same temperatures as the transitions in the high field data in Fig. 6(a). The observation of both transitions in the same low field experiments demonstrates the coexistence of the superconductivity and magnetism.

Resistivity measurements (Fig. 8) show that all samples are metallic ($d\rho/dT>0$) at high temperatures although a semiconducting upturn is observed close to T_c. Superconducting transitions are observed for the $Ru_{1-x}Nb_xSr_2GdCu_2O_8$ solid solutions with $x=0$–0.15 but not for $x=0.2$ down to 7 K. All the $Ru_{1-x}Sn_xSr_2GdCu_2O_8$ samples are superconducting and the onset T_c increases from 38 K to 50 K in the 7.5% Sn sample. The Seebeck coefficient derived from the thermopower

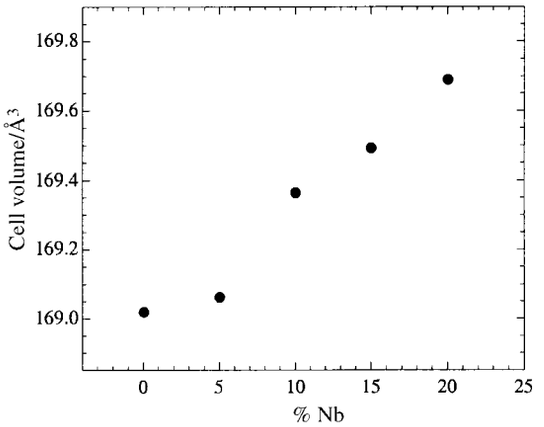

Fig. 4 Variation of the cell volume with x in $Ru_{1-x}Nb_xSr_2GdCu_2O_8$.

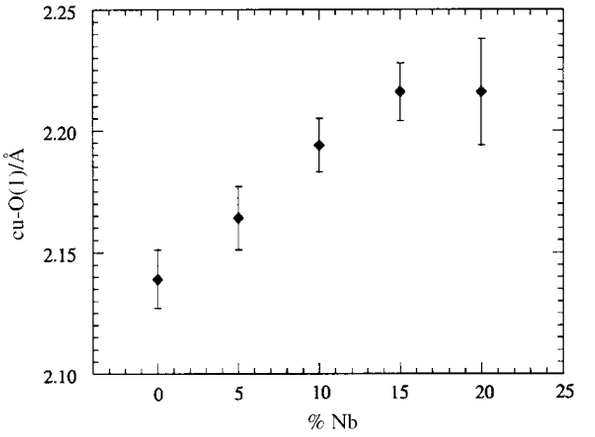

Fig. 5 Changes in the apical Cu–O bond with Nb content in the $Ru_{1-x}Nb_xSr_2GdCu_2O_8$ solid solutions.

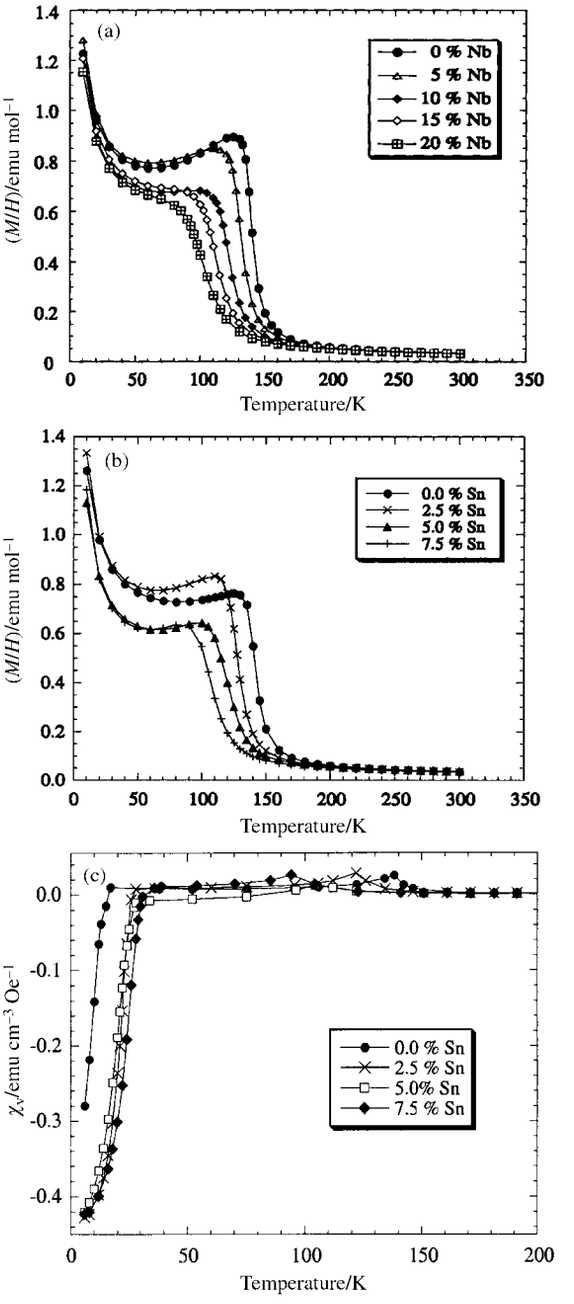

Fig. 6 Magnetisation/field data for $Ru_{1-x}M_xSr_2GdCu_2O_8$ with (a) M = Nb and (b) M = Sn; (c) shows the volume susceptibility for M = Sn at $H=2$ Oe.

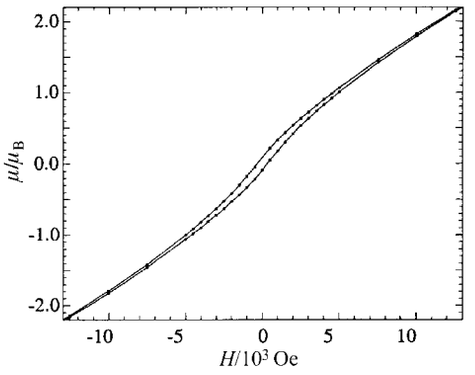

Fig. 7 Magnetic hysteresis loop for $Ru_{0.9}Nb_{0.1}Sr_2GdCu_2O_8$ at 10 K.

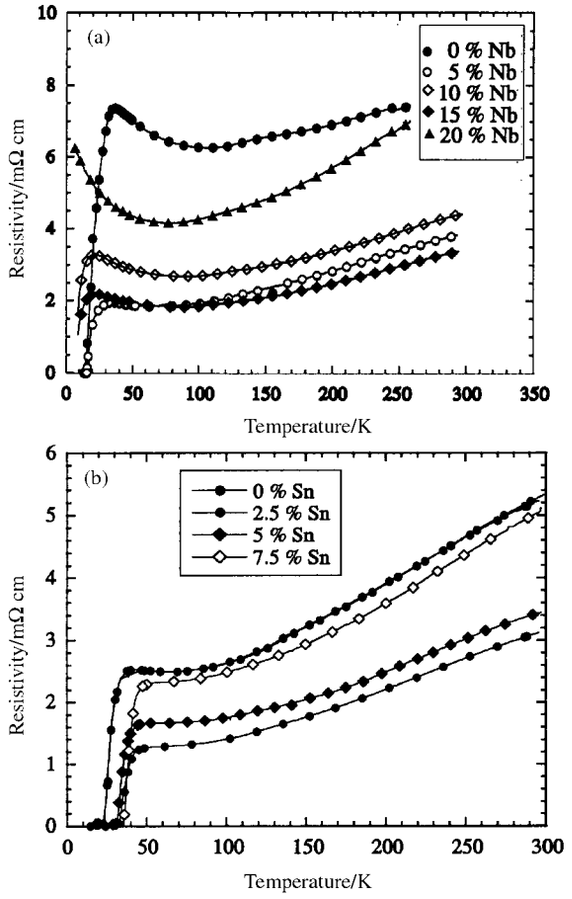

Fig. 8 Resistivity data for $Ru_{1-x}M_xSr_2GdCu_2O_8$ with (a) M = Nb and (b) M = Sn.

measurements increases with x in the Nb doped samples, but decreases in the Sn doped samples (Fig. 9). The Seebeck coefficients are very sensitive to the absolute hole concentrations, and the difference between the values for the $x = 0$ samples in the $Ru_{1-x}Sn_xSr_2GdCu_2O_8$ and $Ru_{1-x}Nb_xSr_2GdCu_2O_8$ series (Table 3) shows that there is a small systematic offset between the doping levels in the two series. This may arise from a small difference in average oxygen contents, below the sensitivity of the thermogravimetric analyses, as the two series were annealed separately.

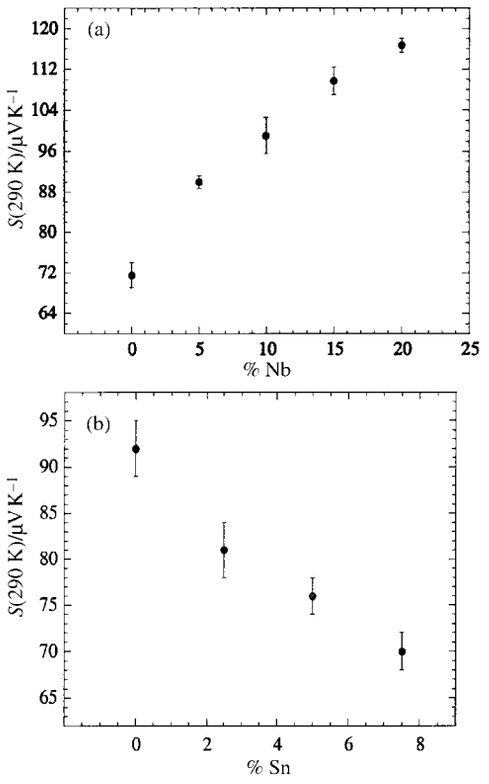

Fig. 9 Variation of the room temperature Seebeck coefficient for $Ru_{1-x}M_xSr_2GdCu_2O_8$ with (a) M = Nb and (b) M = Sn.

Discussion

The crystallographic, magnetic and transport properties evidence the progressive substitution of Ru by M = Nb or Sn in the $Ru_{1-x}M_xSr_2GdCu_2O_8$ solid solutions. The substitution of diamagnetic Sn^{4+} or Nb^{5+} results in a dilution of the ferromagnetism in the Ru–O layers and the Curie temperature, remnant and saturated Ru moments, and coercive field all decrease with x as would be expected.

Both Sn^{4+} and Nb^{5+} are larger than Ru, leading to a slight increase in the average (Ru,M)–O in-plane bond length upon substitution. This increases the bond mismatch between the xy plane Ru–O and Cu–O bonds resulting in greater rotation of the RuO_6 octahedra around c from 15° at $x = 0$ to 17° in the 20% Nb sample (Table 2). The large increase of the apical Cu–

Table 3 Values of the superconducting critical temperature from the onset ($T_{c,onset}$) and zero resistance ($T_{c,0}$) transitions and the onset of diamagnetism ($T_{c,dia}$), the Curie temperature (T_M), coercive field (H_{co}), remnant (μ_R), and saturated (μ_{Ru}) moments per Ru atom, and 290 K thermoelectric powers S_{290} with nominal x and p values for the $Ru_{1-x}M_xSr_2GdCu_2O_8$ (M = Nb, Sn) solid solutions

p	% Nb	% Sn	$T_{c,onset}$/K	$T_{c,0}$/K	$T_{c,dia}$/K	T_M/K	H_{co}/Oe	μ_R/μ_B	μ_{Ru}/μ_B	S_{290}/μV K^{-1}
0.064(5)	20	—	—	—		103(1)	238(1)	0.049(2)	0.59(1)	117(1)
0.068(5)	15	—	19(1)	—		110(1)	295(1)	0.075(1)	0.73(1)	110(3)
0.072(5)	10	—	19(1)	—		118(1)	308(1)	0.086(2)	0.82(1)	99(4)
0.076(5)	5	—	29(1)	15(1)		127(1)	330(1)	0.109(1)	0.94(1)	90(1)
0.080(5)	0	—	37(1)	14(1)		136(1)	405(1)	0.125(1)	0.99(1)	72(2)
0.080(5)	—	0	38(1)	23(1)	17(1)	136(1)	420(1)	0.142(1)	1.09(1)	92(3)
0.091(5)	—	2.5	45(1)	31(1)	28(1)	126(1)	370(1)	0.114(1)	1.00(1)	81(3)
0.101(5)	—	5	46(1)	31(1)	29(1)	117(1)	340(1)	0.096(1)	0.84(1)	76(2)
0.112(5)	—	7.5	50(1)	36(1)	39(1)	103(1)	320(1)	0.088(2)	0.78(1)	70(2)

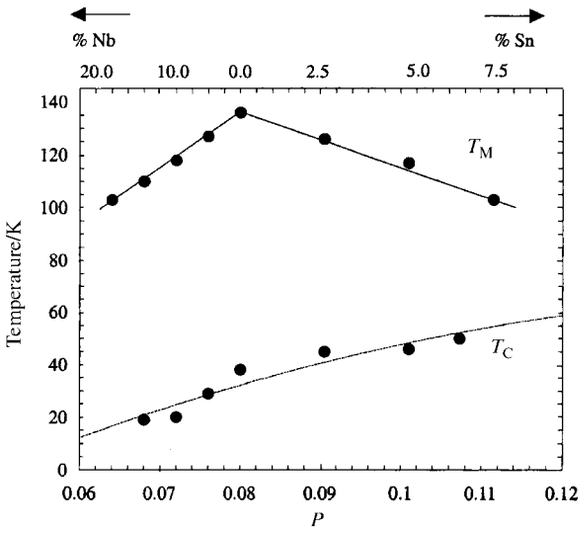

Fig. 10 The variation of the onset superconducting critical temperature (T_c) and the Curie temperature (T_M) with doping level p (lower scale) and % Nb or Sn (upper scale) in the $Ru_{1-x}M_xSr_2GdCu_2O_8$ solid solutions.

O bond from 2.13 Å in the undoped sample to 2.21 Å in $Ru_{0.8}Nb_{0.2}Sr_2GdCu_2O_8$ with a concomitant decrease in the Ru–O apical bonds evidences a reduction in the hole concentration in the CuO_2 planes. Similar results are found during the reduction of $YBa_2Cu_3O_{7-\delta}$[17] as the apical C–O bond increases in length while T_c decreases.

The charge distribution in the doped materials may be written as $(Ru^{5-2p_0})_{1-x}M_x{}^qSr_2Gd(Cu^{2+p_0+\Delta p})_2O_8$ where the extrinsic doping introduced by the substituents M of charge q is $\Delta p=(5-q-2p_0)x/2$, assuming the intrinsic doping level p_0 remains constant. Therefore substitution of $Ru^{(5-2p_0)+}$ by Nb^{5+} leads to the removal of holes from the CuO_2 planes, so that the materials become more underdoped. This is supported by the increase in the 290 K Seebeck coefficient with x in the $Ru_{1-x}Nb_xSr_2GdCu_2O_8$ solid solutions, and the decrease in T_c to 19 K in the 15% Nb sample. The opposite effect occurs upon Sn substitution; the hole concentration increases with a subsequent increase in T_c to 50 K and the Seebeck coefficient decreases. These results provide a good chemical demonstration that the doping of the cuprate planes necessary for superconductivity results from band overlap with the ruthenate states; Sn^{4+} and Nb^{5+} can only have opposite doping effects if the mean Ru oxidation state is intermediate between +4 and +5.

T_c varies quadratically with the hole concentration in cuprates[18] and a fit to the data for the two $Ru_{1-x}M_xSr_2GdCu_2O_8$ series yields values of $p_0=0.08$ for the intrinsic doping level and an estimated maximum T_c of 65 ± 10 K[12] at the optimum $p=0.16$ level. This is much lower than the highest T_c of 105 K obtained for comparable 1212 cuprates such as $(Tl_{0.5}Pb_{0.5})Sr_2(Ca,Y)Cu_2O_7$.[19] This suppression could reflect a pairbreaking interaction with the ferromagnetic moments in the RuO_2 plane, although this effect would be expected to be greater in the undoped compound in which the ferromagnetism is stronger. There is no evidence for this in the data in Fig. 10. The low T_c's in this system may instead reflect lattice strains from the bond mismatch between the cuprate and ruthenate layers. The apical Cu–O bond length of 2.16 Å in $RuSr_2GdCu_2O_8$,[7,11] which is shorter than that in any other cuprate, provides evidence that the geometry of the structure is not optimal for superconductivity.

Acknowledgements

We thank EPSRC for the provision of research grant GR/M59976, ESRF beam time, and a studentship for ACM; I. Pape and A. N. Fitch for help with the synchrotron X-ray diffraction experiment, P. G. Radaelli for assistance with the neutron experiment and S. Rycroft and J. R. Cooper for help with transport measurements.

References

1 W. A. Fertig, D. C. Johnston, L. E. Delong, R. W. McCallum and M. B. Maple, *Phys. Rev. Lett.*, 1977, **38**, 987.
2 L. Bauernfeind, W. Widder and H. F. Braun, *Physica C*, 1995, **254**, 151.
3 K. B. Tang, Y. T. Qian, L. Yang, Y. D. Zhao and Y. H. Zhang, *Physica C*, 1997, **282–287**, 947.
4 I. Felner, U. Asaf, S. Reich and Y. Tsabba, *Physica C*, 1999, **311**, 163.
5 J. L. Tallon, C. Bernhard, M. E. Bowden, P. W. Gilberd, T. M. Stoto and D. J. Pringle, *IEEE Trans. Appl. Supercond.*, 1999, **9**, 1696.
6 C. Bernhard, J. L. Tallon, C. Niedermayer, T. Blasius, A. Golnik, E. Brucher, R. K. Kremer, D. R. Noakes, C. E. Stronach and E. J. Ansaldo, *Phys. Rev. B*, 1999, **59**, 14099.
7 A. C. Mclaughlin, W. Zhou, J. P. Attfield, A. N. Fitch and J. L. Tallon, *Phys. Rev. B*, 1999, **60**, 7512.
8 J. W. Lynn, B. Keimer, C. Ulrich, C. Bernhard and J. L. Tallon, *Phys. Rev. B*, 2000, **61**, 14964.
9 A. C. Mclaughlin, J. P. Attfield and J. L. Tallon, *Int. J. Inorg. Mater.*, 2000, **2**, 95.
10 O. Chmaissam, J. D. Jorgensen, H. Shaked, P. Dollar and J. L. Tallon, *Phys. Rev. B*, 2000, **61**, 6401.
11 A. C. Mclaughlin and J. P. Attfield, *Phys. Rev. B*, 1999, **60**, 14605.
12 A. C. Mclaughlin, V. Janowitz, J. A. McAllister and J. P. Attfield, *Chem. Commun.*, 2000, 1331.
13 A. N. Fitch, *Mater. Sci. Forum*, 1996, **228–231**, 219; J. L. Hodeau, P. Bordet, M. Anne, A. Prat, A. N. Fitch, E. Dooryhee, G. Vaughan and A. Freund, *SPIE Proc.*, 1998, **3448**, 353.
14 S. D. Obertelli, J. R. Cooper and J. L. Tallon, *Phys. Rev. B*, 1992, **46**, 14928.
15 H. M. Rietveld, *Acta Crystallogr.*, 1967, **22**, 151.
16 A. C. Larson and R. B. Von Dreele, Los Alamos National Laboratory Report No. LA-UR-86-748, 1994.
17 R. J. Cava, A. W. Hewat, E. A. Hewat, B. A. Batlogg, M. Marezio, K. M. Rabe, J. J. Krajewski, W. F. Peck Jr. and L. W. Rupp Jr., *Physica C*, 1990, **165**, 419.
18 M. R. Presland, J. L. Tallon, R. G. Buckley, R. S. Liu and N. E. Flower, *Physica C*, 1991, **176**, 95.
19 R. S. Liu, P. P. Edwards, Y. T. Huang, S. F. Wu and P. T. Wu, *J. Solid State Chem.*, 1990, **86**, 334.